SAND2023-05866C

Cramér-Rao Lower Bound for Forced Oscillations under Multi-channel Power Systems Measurements

Z. Xu, J.W. Pierre
Department of Electrical and Computer Engineering
University of Wyoming
Laramie, WY, USA
{zxu3,pierre}@uwyo.edu

R. Elliott, D. Schoenwald, F. Wilches-Bernal, B. Pierre
Electric Power System Research
Sandia National Laboratory
Albuquerque, NM, USA
{rtellio,daschoe,fwilche,bjpierr}@sandia.gov

***Abstract*—The Cramér-Rao Lower Bound (CRLB) is used as a classical benchmark to assess estimators. Online algorithms for estimating modal properties from ambient data, i.e., mode meters, can benefit from accurate estimates of forced oscillations. The CRLB provides insight into how well forced oscillation parameters, e.g., frequency and amplitude, can be estimated. Previous works have solved the lower bound under a single-channel PMU measurement; thus, this paper extends works further to study CRLB under two-channel PMU measurements. The goal is to study how correlated/uncorrelated noise can affect estimation accuracy. Interestingly, these studies shows that correlated noise can decrease the CRLB in some cases. This paper derives the CRLB for the two-channel case and discusses factors that affect the bound.**

I. Introduction

The reliability of electrical power systems is one of the main concerns especially with transmission lines, loads and inter-connecting generators which increase the complexity of analyzing the system. In recent years, synchronized Phasor Measurement Units (PMUs) have been installed across a wide geographical areas to collect current and voltage phasors. These valuable measurements can enhance the reliability of electrical power systems. Since power oscillations are one of the major problems threatening the reliability of wide-area power systems, one application of PMU measurements is to estimate forced oscillations (FOs) parameters, such as frequency, amplitude, etc.

A rogue input driving the system can cause forced oscillations [1], which should be distinguished from electromechanical modal oscillations. Electromechanical modes are properties of the system and excited by continuous random load variations or by sudden system events [2]–[4]; thus its characteristics and consequence to the system are distinct from forced oscillations. Forced oscillations can have large amplitude, and if the frequency of the forced oscillation is near a system modal frequency, forced oscillations can lead to blackouts [5]. However, their sources are not always known. In power systems, forced oscillations may come from steam-turbine regulator malfunction [6], incautious power system stabilizer design [7], or stable limit cycles [8]. Forced oscillations have been observed in PMU data for the US Eastern and Western Interconnects and also the Nordic power system [9].

Forced oscillations can be characterized by their frequency, amplitude, and phase. They can easily be observed in PMU data during times when they have large enough amplitude. Nonetheless, small forced oscillations can be buried under ambient power system noise in many cases because of a small amplitude. Traditional mode meters [2], [10], [11] may give biased mode estimates if the frequency of the forced oscillation is close to the frequency of an electromechanical mode; however this issue is solved by a new class of mode meters [12], [13] which utilize estimates of the forced oscillation frequencies. In addition, these algorithms benefit from highly accurate estimates of frequencies of forced oscillation [14], [15]. Because of the importance of accurate estimation of frequencies of forced oscillations, this research will focus on the ideal achievable estimation. Through all these previous works, the true values of parameters provide a benchmark; but, no research has provided a benchmark for the variance of the parameter estimate. In addition, by all of these estimation algorithms, a variance of estimated parameters are compared with each other, and estimated parameters are close to the true value. However, a lower bound on the variance has not been studied, where such lower bound is called the Cramér-Rao Lower Bound (CRLB).

The previous work [16] has found CRLB for the estimated frequency, amplitude, and phase of forced oscillations when PMU data is collected from a single measurement channel. The goal is to see how the CRLB is decreased by utilizing more than one PMU measurement channel and in particular to gain insight into what influences the CRLB such as the impact of correlation of the noise between the channels, the signal to noise ratio (SNR) of each channel, and the record length. This paper derives closed form expressions for the two PMU channel case that provides these insights.

Notation: The set of integer numbers is denoted by $\mathbb{Z}$. The set of real numbers is denoted by $\mathbb{R}$. A constant or a parameter is indicated by non-bold letters (A, θ). Matrices or vectors are denoted by bold letters ($\boldsymbol{C}$, $\boldsymbol{x}$). In addition, vector transpose $\boldsymbol{\theta}$ is shown as $\boldsymbol{\theta}^\top$ and the N-dimensional identity matrix is denoted by $\boldsymbol{I}_{N\times N}$.

The paper is organized in the following: Section II provides details about the modeling of a forced oscillation in PMU data under a two-measurement channel. In Section III, a direct

978-1-6654-1211-7/22/ $31.00 ©2022 IEEE

method to solve the CRLB of forced oscillation's amplitude, phase, and frequency is derived. Section IV discusses the CRLB for the estimated frequency, amplitude, and phase of forced oscillations under specifics situation. Section V gives the conclusions of the paper.

II. Mathematical Model

If a forced oscillation (FO) appears in PMU measurements of power systems, each channel of sampled measurement data can be written as the sum of ambient power system noise and the forced oscillation,

$$x_i[n] = s_i[n] + w_i[n], n = 0, 1, \ldots, (N-1), \tag{1}$$

where $i \in \mathbb{Z}^+$ denotes the ith channel in PMU measurements. The FO signal in the ith channel is expressed as $s_i[n]$, and N is the length of the measurement window. To keep the mathematics tractable, the noise in each channel is modeled as white Gaussian noise but the noise between the channels can be correlated. This is often referred to as temporally white but spatially correlated. This model for the noise will lead to gaining insight into the effect spatial correlation has on the CRLB. As in [17], the appearance of FOs in PMU measurements can be modeled as sinusoidal which can be written as

$$s_i[n, \boldsymbol{\theta}_i] = A_i \cos(2\pi f_0 n + \phi_i), \tag{2}$$

where $A_i \in \mathbb{R}$ is the amplitude of the FO in the ith channel, and $f_0 \in [0, 1]$ is the normalized frequency of the FO (i.e. $f_0 = F_0/F_s$) where F_0, with unit Hz (cycles per second), is the real frequency of the FO, and F_s is the sampling frequency of PMU with units of samples per second. The phase of the FO is $\phi_i \in [-\pi, \pi]$ in units of radians for the ith channel. Amplitudes, phases, and frequencies are all unknown parameters that need to be estimated.

Here, to keep the mathematics tractable and to gain the desired insight, just two channels are considered as shown in Fig. 1. The final two-channel measurement vector can be written as

$$\boldsymbol{x} = \begin{bmatrix} \boldsymbol{x}_1 \\ \boldsymbol{x}_2 \end{bmatrix} = \underbrace{\begin{bmatrix} A_1 \cos\phi_1 \\ A_1 \cos(2\pi f_0 + \phi_1) \\ A_1 \cos(2\pi 2 f_0 + \phi_1) \\ \vdots \\ A_1 \cos(2\pi (N-1) f_0 + \phi_1) \\ A_2 \cos\phi_2 \\ A_2 \cos(2\pi f_0 + \phi_2) \\ A_2 \cos(2\pi 2 f_0 + \phi_2) \\ \vdots \\ A_2 \cos(2\pi (N-1) f_0 + \phi_2) \end{bmatrix}}_{\boldsymbol{s} = \begin{bmatrix} \boldsymbol{s}_1 \\ \boldsymbol{s}_2 \end{bmatrix}} + \underbrace{\begin{bmatrix} w_1[0] \\ w_1[1] \\ w_1[2] \\ \vdots \\ w_1[N-1] \\ w_2[0] \\ w_2[1] \\ w_2[2] \\ \vdots \\ w_2[N-1] \end{bmatrix}}_{\boldsymbol{w} = \begin{bmatrix} \boldsymbol{w}_1 \\ \boldsymbol{w}_2 \end{bmatrix}}, \tag{3}$$

where the unknown parameter vector is $\boldsymbol{\theta} = [A_1\, A_2\, \phi_1\, \phi_2\, f_0]^\top$.

In this section, the two-channel PMU measurement case is explored. A variety of approaches in previous works [12], [13], [17]–[21] has been provided to estimate unknown parameters in FO; nevertheless, this paper aims to solve the lowest variance of unknown parameters in FO, which previous works have not addressed. In the next section, the lowest variance will be solved.

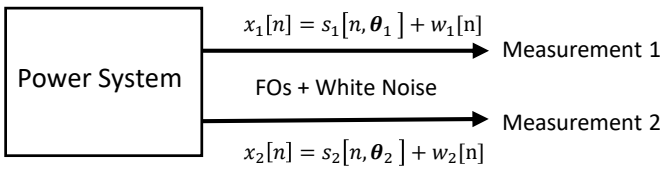

Fig. 1. System sketch for two channels PMU measurements

III. Cramér-Rao Lower Bound

Cramér-Rao Lower Bound (CRLB) is a lower bound on the variance of any unbiased estimator which, if achievable, is the smallest possible variance; however, in practice, many unbiased estimators cannot achieve this bound. Thus, the bound can provide a benchmark to assess different estimator performances. The CRLB is not connected to a particular estimation method or whether the data is being analyzed in the time or frequency domain, but is fundamental to the problem. Given the CRLB theorem in [22], the CRLB is found by first finding the Fisher information matrix and then taking its inverse. Finally, the diagonal elements at the inverse Fisher information matrix are taken as lower bounds. Additionally, the closed-form expressions for the CRLBs need to be analyzed to gain insight into what influences estimation accuracy.

A. Solving Fisher information matrix

To solve the CRLB, the Fisher information matrix needs to be found. In this paper, the amplitudes, phases, and frequency are the unknown parameters, $\boldsymbol{\theta} = [A_1, A_2, \phi_1, \phi_2, f_0]^\top$. The Fisher information matrix $\boldsymbol{I}(\boldsymbol{\theta})$ can be defined as a 5×5 matrix, and each entry in the matrix $\boldsymbol{I}(\boldsymbol{\theta})$ can be solved as

$$[\boldsymbol{I}(\boldsymbol{\theta})]_{ij} = -\mathrm{E}\left[\frac{\partial^2 \ln p[\boldsymbol{x}, \boldsymbol{\theta}]}{\partial\theta_i \partial\theta_j}\right], \tag{4}$$

where $i, j \in \{1, 2, \ldots, 5\}$, and $[\cdot]_{ij}$ stands for the element at the ith column and jth row of the matrix. The signal $\boldsymbol{x}$ has been defined in (3); since $\boldsymbol{w}$ is Gaussian noise, the probability density function (PDF) of output $\boldsymbol{x}$ is solved as

$$p(\boldsymbol{x}; \boldsymbol{\theta}) = \frac{1}{(2\pi)^{\frac{N}{2}} \det(\boldsymbol{C})^{\frac{1}{2}}} \exp\left\{\frac{1}{2}(\boldsymbol{x} - s(\boldsymbol{\theta}))^\top \boldsymbol{C}^{-1}(\boldsymbol{x} - s(\boldsymbol{\theta}))\right\}, \tag{5}$$

where $\boldsymbol{C} \in \mathbb{R}_{2N \times 2N}$ is the covariance matrix of the noise $\boldsymbol{w}$, which can be solved as

$$\boldsymbol{C} = \mathrm{E}\left\{\begin{bmatrix} w_1[0]w_1[0] & w_1[0]w_1[1] & \ldots & w_1[0]w_2[N-1] \\ w_1[1]w_1[0] & w_1[1]w_1[1] & \ldots & w_1[1]w_2[N-1] \\ \vdots & \vdots & \ddots & \vdots \\ w_2[N-1]w_1[0] & w_2[N-1]w_1[1] & \ldots & w_2[N-1]w_2[N-1] \end{bmatrix}\right\}, \tag{6}$$

and $\det(\boldsymbol{C})$ denotes the determinant of the matrix $\boldsymbol{C}$. Since $\boldsymbol{w}_1$ and $\boldsymbol{w}_2$ are temporally white but spatially correlated,

the covariance matrix can be expressed by the correlation coefficient ρ in (7). Step details to find this are given in Section A of the Appendix.

$$\boldsymbol{C} = \begin{bmatrix} \gamma_1 \boldsymbol{I} & \gamma_{12}\boldsymbol{I} \\ \gamma_{21}\boldsymbol{I} & \gamma_2 \boldsymbol{I} \end{bmatrix} = \begin{bmatrix} \sigma_1^2 \boldsymbol{I} & \rho\sigma_1\sigma_2 \boldsymbol{I} \\ \rho\sigma_1\sigma_2 \boldsymbol{I} & \sigma_2^2 \boldsymbol{I} \end{bmatrix} \tag{7}$$

where σ_1^2 and σ_2^2 are the variance of $\boldsymbol{w_1}$ and $\boldsymbol{w_2}$, respectively. In addition, $\boldsymbol{I}$ stands for identity matrix. Substitute (5) into (4), one can simplify the Fisher information matrix as

$$[\boldsymbol{I}(\boldsymbol{\theta})]_{ij} = \left[\frac{\partial s(\boldsymbol{\theta})}{\partial \theta_i}\right]^\top \boldsymbol{C}^{-1} \left[\frac{\partial s(\boldsymbol{\theta})}{\partial \theta_j}\right], \tag{8}$$

where partial derivatives for each parameter are

$$\frac{\partial \boldsymbol{s}(\boldsymbol{\theta})}{\partial \theta_1} = \begin{bmatrix} \cos\phi_1 \\ \cos(2\pi f_0 + \phi_1) \\ \cos(4\pi f_0 + \phi_1) \\ \vdots \\ \cos(2(N-1)\pi f_0 + \phi_1) \\ 0 \\ 0 \\ \vdots \\ 0 \end{bmatrix}, \frac{\partial \boldsymbol{s}(\boldsymbol{\theta})}{\partial \theta_2} = \begin{bmatrix} 0 \\ 0 \\ \vdots \\ 0 \\ \cos\phi_2 \\ \cos(2\pi f_0 + \phi_2) \\ \cos(4\pi f_0 + \phi_2) \\ \vdots \\ \cos(2(N-1)\pi f_0 + \phi_2) \end{bmatrix}, \tag{9}$$

$$\frac{\partial \boldsymbol{s}(\boldsymbol{\theta})}{\partial \theta_3} = \begin{bmatrix} -A_1\sin(\phi_1) \\ -A_1\sin(2\pi f_0 + \phi_1) \\ -A_1\sin(4\pi f_0 + \phi_1) \\ \vdots \\ -A_1\sin(2(N-1)\pi f_0 + \phi_1) \\ 0 \\ 0 \\ \vdots \\ 0 \end{bmatrix}, \frac{\partial \boldsymbol{s}(\boldsymbol{\theta})}{\partial \theta_4} = \begin{bmatrix} 0 \\ 0 \\ \vdots \\ 0 \\ -A_2\sin(\phi_2) \\ -A_1\sin(2\pi f_0 + \phi_2) \\ -A_1\sin(4\pi f_0 + \phi_2) \\ \vdots \\ -A_2\sin(2(N-1)\pi f_0 + \phi_2) \end{bmatrix}, \tag{10}$$

$$\frac{\partial \boldsymbol{s}(\boldsymbol{\theta})}{\partial \theta_5} = \begin{bmatrix} 0 \\ -A_1 2\pi\sin(2\pi f_0 + \phi_1) \\ -A_1 4\pi\sin(4\pi f_0 + \phi_1) \\ \vdots \\ -A_1 2(N-1)\pi\sin(2(N-1)\pi f_0 + \phi_1) \\ 0 \\ -A_2 2\pi\sin(2\pi f_0 + \phi_2) \\ -A_2 4\pi\sin(4\pi f_0 + \phi_2) \\ \vdots \\ -A_2 2(N-1)\pi\sin(2(N-1)\pi f_0 + \phi_2) \end{bmatrix}. \tag{11}$$

In Section B of the Appendix, the elements of the Fisher information matrix are then found using (7–11). The Fisher information matrix can finally be expressed as (12). For concise expression, a_1, a_2, a_3, b_1 and b_2 are used in the (12), where $a_1 = \frac{1}{\sigma_1^2(1-\rho^2)}$,$a_2 = \frac{1}{\sigma_2^2(1-\rho^2)}$,$a_3 = \frac{1}{\sigma_1\sigma_2(1-\rho^2)}$, $b_1 = \cos(\phi_1 - \phi_2)$, and $b_2 = \sin(\phi_1 - \phi_2)$.

B. Solving for the CRLB

By applying the CRLB theorem [22], the true value of the estimation parameter is used; the CRLB of a parameter is the diagonal element of the inverse of the Fisher information matrix

$$\text{Var}(\hat{\theta}_i) \geq \left[\boldsymbol{I}^{-1}(\boldsymbol{\theta})\right]_{ii}, \tag{13}$$

where $i = 1, 2, \ldots 5$, and $\boldsymbol{I}^{-1}(\boldsymbol{\theta}) \in \mathbb{R}_{5\times 5}$ is inverse of Fisher information matrix given in (12). Var $(\hat{\theta}_i)$ is to place a bound on the variance of the estimate of the ith parameter in $\boldsymbol{\theta}$.

Finally, the CRLB of amplitude, phase and frequency are solved as

$$\text{Var}(\hat{A}_1) \geq \frac{2\sigma_1^2}{N}, \tag{14}$$

$$\text{Var}(\hat{A}_2) \geq \frac{2\sigma_2^2}{N}, \tag{15}$$

$$\text{Var}(\hat{\phi}_1) \geq \frac{1}{N\eta_1} + \frac{(N-1)}{N(N+1)}\frac{3(1-\rho^2)}{\eta_1 + \eta_2 - 2\rho b_1\sqrt{\eta_1\eta_2}}, \tag{16}$$

$$\text{Var}(\hat{\phi}_2) \geq \frac{1}{N\eta_2} + \frac{(N-1)}{N(N+1)}\frac{3(1-\rho^2)}{\eta_1 + \eta_2 - 2\rho b_1\sqrt{\eta_1\eta_2}}, \tag{17}$$

$$\text{Var}(\hat{F}_0) \geq \frac{12F_s^2}{(2\pi)^2 N(N^2-1)}\frac{(1-\rho^2)}{\eta_1 + \eta_2 - 2\rho b_1\sqrt{\eta_1\eta_2}}, \tag{18}$$

where η_i is the signal-to-noise ratio (SNR), which is defined as the mean square value of the FO in the ith channel divided by the ambient noise power in the ith channel,

$$\eta_i = \frac{A_i^2/2}{\sigma_i^2}. \tag{19}$$

The above closed-form solutions give key insights into what are important factors when estimating the amplitudes, phases, and frequencies of forced oscillations. For instance: The CRLB for the amplitude estimate is directly proportional to the value of noise power σ_i^2, and inversely proportional to the number of samples (N). Intuitively, as the noise power increases, one could get worse estimation results. If the length of estimation data increases, which means more achievable information of FOs, the estimation accuracy highly increases. Compared to CRLB for the phase or the frequency, one can obviously observe that CRLB for the amplitude is only determined by two main factors; thus, discussions will mainly focus on CRLB for the phase or the frequency in the next section.

This section completely described deriving the CRLB and arriving at a closed-form expression for each of the estimated unknown parameters. In the result section to follow, a closer look will be made regarding the closed-form expressions for the CRLB of the phase and frequency estimates to gain more intuitive insight into what influences the estimation of these parameters.

IV. Results and Discussions

The closed-form expressions of the CRLB for the phase and frequency are complicated expressions and are hard for the reader to easily find insight to discover how the lower bounds are affected by different parameters. Here, three different cases will be discussed to help the reader understand CRLB for the phase and the frequency.

$$I(\boldsymbol{\theta}) = \begin{bmatrix} \frac{N}{2}a_1 & \frac{N}{2}a_3b_1 & 0 & \frac{N}{2}a_3A_2b_2 & \frac{N(N-1)}{2}\pi a_3A_2b_2 \\ \frac{N}{2}a_3b_1 & \frac{N}{2}a_2 & \frac{N}{2}a_3A_1b_2 & 0 & -\frac{N(N-1)}{2}\pi a_3A_1b_2 \\ 0 & \frac{N}{2}a_3A_1b_2 & \frac{N}{2}a_1A_1^2 & \frac{N}{2}a_3A_1A_2b_1 & \frac{N(N-1)}{2}\pi(a_1A_1^2 + a_3A_1A_2b_2) \\ -\frac{N}{2}a_3A_2b_2 & 0 & \frac{N}{2}a_3A_1A_2b_1 & \frac{N}{2}a_2A_2^2 & \frac{N(N-1)}{2}\pi(a_2A_2^2 + a_3A_1A_2b_2) \\ \frac{N(N-1)}{2}\pi a_3A_2b_2 & -\frac{N(N-1)}{2}\pi a_3A_1b_2 & \frac{N(N-1)}{2}\pi(a_1A_1^2 + a_3A_1A_2b_2) & \frac{N(N-1)}{2}\pi(a_2A_2^2 + a_3A_1A_2b_2) & \frac{N(N-1)(2N-1)}{6}\frac{(2\pi^2)}{2}(a_1A_1^2 + a_2A_2^2 + 2a_3A_1A_2b_1) \end{bmatrix} \tag{12}$$

A. Perfect Correlation

Under the perfect correlation case, the noise in the two channels is the same to within a constant multiplier. The value of correlation coefficient is $\rho = 1$ or -1; thus, the CRLB in (16), (17) and (18) become

$$\text{Var}\,(\hat{\phi_1}) \geq \frac{1}{N\eta_1}, \tag{20}$$

$$\text{Var}\,(\hat{\phi_2}) \geq \frac{1}{N\eta_2}, \tag{21}$$

$$\text{Var}\,(\hat{F_0}) \geq 0. \tag{22}$$

Interestingly, the CRLB for the frequency is equal to 0, which means the lower bound on the variance of the frequency estimate is zero. The CRLB for the phase is inversely proportional to the SNR η_i, and inversely proportional to the number of samples (N). Compared with the CRLB of single channel PMU measurement in [22], the CRLB for the phase under two channels PMU measurement is 4 times smaller than the single channel case for large N.

B. No Correlation

This subsection aims to examine how estimation accuracy changes if the noise in two measurement channels is uncorrelated. As $\boldsymbol{w_1}$ and $\boldsymbol{w_2}$ are uncorrelated, the value of the correlation coefficient is $\rho = 0$. The CRLB in (16), (17) and (18) can be simplified as

$$\text{Var}\,(\hat{\phi_1}) \geq \frac{1}{N\eta_1} + \frac{(N-1)}{N(N+1)}\frac{3}{\eta}, \tag{23}$$

$$\text{Var}\,(\hat{\phi_2}) \geq \frac{1}{N\eta_2} + \frac{(N-1)}{N(N+1)}\frac{3}{\eta}, \tag{24}$$

$$\text{Var}\,(\hat{F_0}) \geq \frac{12F_s^2}{(2\pi)^2N(N^2-1)}\frac{1}{\eta}, \tag{25}$$

where $\eta = \eta_1 + \eta_2$ is defined as total SNR of the system. From the above three equations, one can observe

- The CRLB for the phase is inversely proportional to the number of samples (N); in addition, it also has a term inversely proportional to the total SNR (η) and a term inversely proportional to the SNR at that channel. One thing should be noticed here if $\eta_1 = 0$ or $\eta_2 = 0$ which means only one signal presence in the measurement; in other words, this case can be considered as a single channel PMU measurement. The CRLB is simplified as

$$\text{Var}\,(\hat{\phi_i}) \geq \frac{2(2N-1)}{N(N+1)\eta_i}. \tag{26}$$

  The above results exactly match the result in [22], and (23), (24) guarantee to be smaller than the single channel case in (26) for large N.
- The CRLB for the frequency is inversely proportional to total SNR (η). But the bound falls off much more quickly with the number of samples since it is inversely proportional to N^3 for the bound on the frequency compared to N for the amplitude and the phase. If $\eta_1 = 0$ or $\eta_2 = 0$, the CRLB is simplified as

$$\text{Var}\,(\hat{F_0}) \geq \frac{12F_s^2}{(2\pi)^2N(N^2-1)\eta_i}, \tag{27}$$

  where the above result also matches results in [22]. Compared to (25) and (27), one can notice that the CRLB for the frequency in the multi-channel case is smaller than the single-channel case because of total SNR in (25).

C. Correlated channel

As previous two subsections discuss some special cases of the value of the correlation coefficient. This section will focus on when $0 < |\rho| < 1$.

It is easy to observe from (16–18) that the CRLB for the phase is inversely proportional to the number of samples (N), and the CRLB for the frequency is inversely proportional to N^3. It is also clear that the bounds decrease with increasing SNRs. The other two parameters that play key roles in the bounds are the correlation coefficient (ρ) and b_1 which is the cosine of the phase angle difference. Note, both these values are constrained to be between -1 and 1. Since cosine is an even function, the bounds are an even function of the phase angle difference. Notice that the CRLB for the phase has two terms, where the first term is inversely proportional to N and the channel's SNR but does not depend on ρ or b_1. The second term, and also the CRLB for the frequency, depends on the two SNRs, ρ, and b_1. Because of the $(1-\rho^2)$, this goes to zero if $|\rho| = 1$. Also, b_1 only appears in the expression as

a product with ρ, where ρb_1 is between -1 and 1. So if that product is negative it increases the size of the denominator and thus decreases the bound. If that product is positive the opposite is true. Two figures are given to better understand the variation of the CRLB as phase difference and correlation coefficient change. In the first case, the phase difference is fixed at $\pi/3$. For other parameters, $\eta_1 = \eta_2 = 5\text{dB}$, $N = 100$, $F_s = 5$. Fig. 2(a) shows that when ρ increases, the CRLB for both phase and frequency has a similar U-shape, where ρ can be determined to find the maximum value for the CRLB. In the second case, ρ is fixed at a value 0.2, and other parameters' values are as same as before. From Fig. 2(b), the CRLB for the phase or the frequency has a similar U-shape and the maximum CRLB value is at phase difference 0. If ρ is positive, the CRLB for the phase or the frequency is monotonically decreasing as the phase difference goes from 0 to π. But if ρ is negative, the CRLB for the phase or the frequency is monotonically increasing. In addition, one can observe that curve of the CRLB for the frequency falls off faster than the phase, which is mentioned in the earlier section. From the discussions in this section, correlated noise can improve potential estimation accuracy under some situations by decreasing the bound.

V. Conclusion

This paper proposes the mathematical model of FOs in two-PMU measurement channels, and instead of focusing on estimating parameters in FOs, this paper solves for a bound on the achievable estimation performance. Such a bound acts as a benchmark to evaluate different estimation algorithms. Cramér-Rao Lower Bound, known as a classic benchmark, is introduced and solved. The closed form of the CRLB gives readers insightful perspectives to view different kinds of parameters affecting estimation accuracy. Additionally, this paper explores how noise in two different channels affects the CRLB of unknown parameters in FOs. Future work will study FOs under colored Gaussian noise instead of white Gaussian noise, accurately describing the ambient power system.

Acknowledgment

This work was supported by the U.S. Department of Energy Office of Electricity Advanced Modeling Grid Research Program led by Dr. Ali Ghassemian.

Sandia National Laboratories is a multi-mission laboratory managed and operated by National Technology and Engineering Solutions of Sandia, LLC., a wholly owned subsidiary of Honeywell International, Inc., for the U.S. Department of Energy's National Nuclear Security Administration under contract DE-NA-0003525.

Appendix

A. Solving Covariance Matrix

As shown in (3), the noise part can be written as vector form as $\boldsymbol{w} = [\boldsymbol{w_1}^\top \quad \boldsymbol{w_2}^\top]^\top$. Thus, given (6), the covariance matrix can rewrite as,

$$\boldsymbol{C} = E\{\boldsymbol{w}\boldsymbol{w}^\top\} = E\left\{\begin{bmatrix}\boldsymbol{w_1}\\ \boldsymbol{w_2}\end{bmatrix}\begin{bmatrix}\boldsymbol{w_1}^\top & \boldsymbol{w_2}^\top\end{bmatrix}\right\}, \tag{28}$$

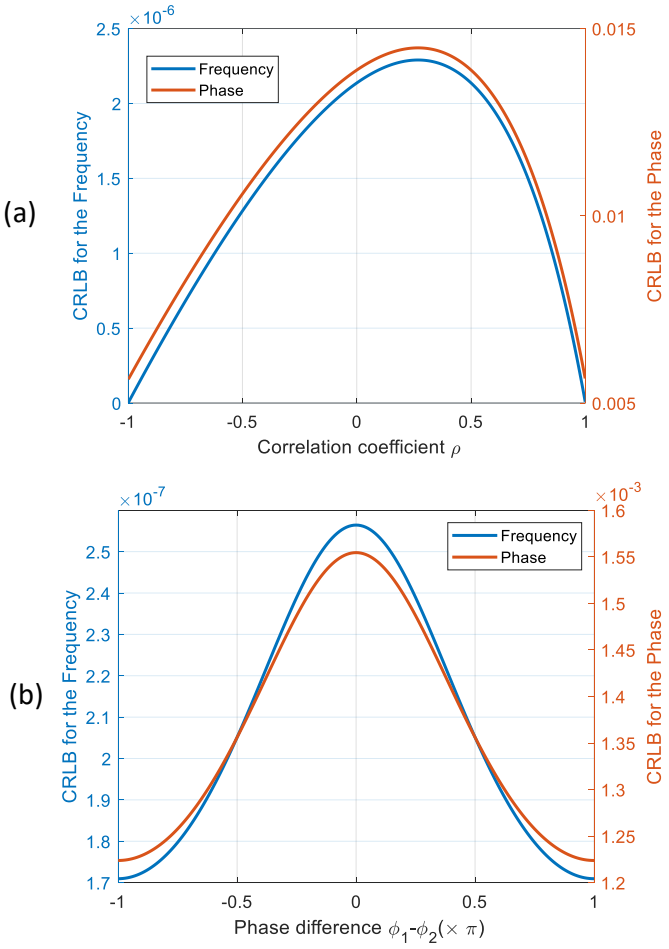

Fig. 2. CRLB for the frequency and the phase as correlation coefficient or phase change. The range of x-axis in (b) is $[-\pi, \pi]$, which has been scaled by π to $[-1, 1]$.

which is simplified as

$$\boldsymbol{C} = \begin{bmatrix}E\{\boldsymbol{w_1}\boldsymbol{w_1}^\top\} & E\{\boldsymbol{w_1}\boldsymbol{w_2}^\top\}\\ E\{\boldsymbol{w_2}\boldsymbol{w_1}^\top\} & E\{\boldsymbol{w_2}\boldsymbol{w_2}^\top\}\end{bmatrix}. \tag{29}$$

Since, $\boldsymbol{w_1}$ and $\boldsymbol{w_2}$ are assumed to be white Gaussian noise with mean of 0 and variance of σ_1^2, σ_2^2, respectively. Thus, one can rewrite covariance matrix as

$$\boldsymbol{C} = \begin{bmatrix}\gamma_1\boldsymbol{I} & \gamma_{12}\boldsymbol{I}\\ \gamma_{21}\boldsymbol{I} & \gamma_2\boldsymbol{I}\end{bmatrix}. \tag{30}$$

Based on the characteristics of white Gaussian noise $\boldsymbol{w_1}$ and $\boldsymbol{w_2}$

$$E\{\boldsymbol{w_i}\boldsymbol{w_i}^\top\} = \sigma_i^2\boldsymbol{I} = \gamma_i\boldsymbol{I}, \tag{31}$$

where $i = 1$ or $i = 2$, If $\boldsymbol{w_1}$ and $\boldsymbol{w_2}$ are independent of each other, one can find that $E\{\boldsymbol{w_1}\boldsymbol{w_2}^\top\} = 0$; however, here, $\boldsymbol{w_1}$ and $\boldsymbol{w_2}$ are considered as more general case: if $\boldsymbol{w_1}$ and $\boldsymbol{w_2}$ are assumed to be correlated with each other with correlation coefficient ρ. Thereby, $\rho = \frac{\gamma_{12}}{\sqrt{\gamma_1}\sqrt{\gamma_2}} = \frac{\gamma_{12}}{\sqrt{\sigma_1}\sqrt{\sigma_2}}$ Finally, one

can get $\gamma_{12} = \gamma_{21} = \rho\sigma_1\sigma_2$. The covariance matrix can be expressed as

$$\boldsymbol{C} = \begin{bmatrix} \sigma_1^2 I & \rho\sigma_1\sigma_2 I \\ \rho\sigma_1\sigma_2 I & \sigma_2^2 I \end{bmatrix}. \tag{32}$$

B. Solving Fisher Information Matrix

$$[\boldsymbol{I}(\boldsymbol{\theta})]_{11} = \frac{1}{\sigma_1^2\sigma_2^2(1-\rho^2)}\left(\frac{N\sigma_2^2}{2} - 0 - 0 + 0\right) = \frac{N}{2\sigma_1^2(1-\rho^2)} \tag{33}$$

$$[\boldsymbol{I}(\boldsymbol{\theta})]_{12} = \frac{1}{\sigma_1^2\sigma_2^2(1-\rho^2)}\left(0 - 0 - \frac{N\rho\sigma_1\sigma_2\cos(\phi_1-\phi_2)}{2}\right) \tag{34}$$

$$[\boldsymbol{I}(\boldsymbol{\theta})]_{13} = \frac{1}{\sigma_1^2\sigma_2^2(1-\rho^2)}(0 - 0 - 0 + 0) = 0 \tag{35}$$

$$[\boldsymbol{I}(\boldsymbol{\theta})]_{14} = \frac{1}{\sigma_1^2\sigma_2^2(1-\rho^2)}\left(0 - 0 - \frac{NA_2\rho\sigma_1\sigma_2\sin(\phi_1-\phi_2)}{2}\right) \tag{36}$$

$$[\boldsymbol{I}(\boldsymbol{\theta})]_{15} = \frac{N\pi A_2\rho\sigma_1\sigma_2\sin(\phi_1-\phi_2)}{\sigma_1^2\sigma_2^2(1-\rho^2)}\sum_{n=0}^{N-1} n \tag{37}$$

$$[\boldsymbol{I}(\boldsymbol{\theta})]_{22} = \frac{1}{\sigma_1^2\sigma_2^2(1-\rho^2)}\left(0 - 0 - 0 + \frac{N\sigma_1^2}{2}\right) \tag{38}$$

$$[\boldsymbol{I}(\boldsymbol{\theta})]_{23} = \frac{\frac{N}{2}\pi A_1\rho\sigma_1\sigma_2\sin(\phi_1-\phi_2)}{\sigma_1^2\sigma_2^2(1-\rho^2)} \tag{39}$$

$$[\boldsymbol{I}(\boldsymbol{\theta})]_{24} = \frac{1}{\sigma_1^2\sigma_2^2(1-\rho^2)}(0 - 0 - 0 + 0) = 0 \tag{40}$$

$$[\boldsymbol{I}(\boldsymbol{\theta})]_{25} = \frac{N\pi A_1\rho\sigma_1\sigma_2\sin(\phi_1-\phi_2)}{\sigma_1^2\sigma_2^2(1-\rho^2)}\sum_{n=0}^{N-1} n \tag{41}$$

$$[\boldsymbol{I}(\boldsymbol{\theta})]_{33} = \frac{1}{\sigma_1^2\sigma_2^2(1-\rho^2)}\left(\frac{N\sigma_1^2A_1^2}{2} - 0 - 0 + 0\right) \tag{42}$$

$$[\boldsymbol{I}(\boldsymbol{\theta})]_{34} = \frac{\frac{N}{2}A_1A_2\rho\sigma_1\sigma_2\cos(\phi_1-\phi_2)}{\sigma_1^2\sigma_2^2(1-\rho^2)} \tag{43}$$

$$[\boldsymbol{I}(\boldsymbol{\theta})]_{35} = \frac{(\sigma_2^2A_1^2 - \rho\sigma_1\sigma_2A_1A_2\cos(\phi_1-\phi_2))\pi}{\sigma_1^2\sigma_2^2(1-\rho^2)}\sum_{n=0}^{N-1} n \tag{44}$$

$$[\boldsymbol{I}(\boldsymbol{\theta})]_{44} = \frac{1}{\sigma_1^2\sigma_2^2(1-\rho^2)}\left(0 - 0 - 0 + \frac{N\sigma_1^2A_2^2}{2}\right) \tag{45}$$

$$[\boldsymbol{I}(\boldsymbol{\theta})]_{45} = \frac{(\sigma_1^2A_2^2 - \rho\sigma_1\sigma_2A_1A_2\cos(\phi_1-\phi_2))\pi}{\sigma_1^2\sigma_2^2(1-\rho^2)}\sum_{n=0}^{N-1} n \tag{46}$$

$$[\boldsymbol{I}(\boldsymbol{\theta})]_{55} = \frac{(\sigma_1^2A_2^2 + \sigma_2^2A_1^2 - 2\rho\sigma_1\sigma_2A_1A_2\cos(\phi_1-\phi_2))2\pi}{\sigma_1^2\sigma_2^2(1-\rho^2)}\sum_{n=0}^{N-1} n^2 \tag{47}$$

REFERENCES

[1] J. Follum and J. W. Pierre, "Initial results in the detection and estimation of forced oscillations in power systems," in *2013 North American Power Symposium (NAPS)*. IEEE, 2013, pp. 1–6.

[2] R. W. Wies, J. W. Pierre, and D. J. Trudnowski, "Use of arma block processing for estimating stationary low-frequency electromechanical modes of power systems," *IEEE Transactions on Power Systems*, vol. 18, no. 1, pp. 167–173, 2003.

[3] M. A. Khan, J. W. Pierre, D. J. Trudnowski, and S. S. Wulff, "An initial study of ambient noise in synchrophasor measurements," in *2016 North American Power Symposium (NAPS)*. IEEE, 2016, pp. 1–6.

[4] J. Follum, F. Tuffner, and U. Agrawal, "Applications of a new nonparametric estimator of ambient power system spectra for measurements containing forced oscillations," in *2017 IEEE Power & Energy Society General Meeting*. IEEE, 2017, pp. 1–5.

[5] H. Ye, Y. Liu, P. Zhang, and Z. Du, "Analysis and detection of forced oscillation in power system," *IEEE Transactions on Power Systems*, vol. 32, no. 2, pp. 1149–1160, 2016.

[6] W. Xuanyin, L. Xiaoxiao, and L. Fushang, "Analysis on oscillation in electro-hydraulic regulating system of steam turbine and fault diagnosis based on psobp," *Expert Systems with Applications*, vol. 37, no. 5, pp. 3887–3892, 2010.

[7] M. Magdy and F. Coowar, "Frequency domain analysis of power system forced oscillations," in *IEE proceedings C (Generation, transmission and distribution)*, vol. 137, no. 4. IET, 1990, pp. 261–268.

[8] P. B. Reddy and I. A. Hiskens, *Limit-induced stable limit cycles in power systems*. IEEE, 2005.

[9] L. Vanfretti, L. Dosiek, J. W. Pierre, D. Trudnowski, J. H. Chow, R. García-Valle, and U. Aliyu, "Application of ambient analysis techniques for the estimation of electromechanical oscillations from measured pmu data in four different power systems," *European Transactions on Electrical Power*, vol. 21, no. 4, pp. 1640–1656, 2011.

[10] J. W. Pierre, D. J. Trudnowski, and M. K. Donnelly, "Initial results in electromechanical mode identification from ambient data," *IEEE Transactions on Power Systems*, vol. 12, no. 3, pp. 1245–1251, 1997.

[11] D. J. Trudnowski, J. W. Pierre, N. Zhou, J. F. Hauer, and M. Parashar, "Performance of three mode-meter block-processing algorithms for automated dynamic stability assessment," *IEEE Transactions on Power Systems*, vol. 23, no. 2, pp. 680–690, 2008.

[12] J. Follum, J. W. Pierre, and R. Martin, "Simultaneous estimation of electromechanical modes and forced oscillations," *IEEE Transactions on Power Systems*, vol. 32, no. 5, pp. 3958–3967, 2016.

[13] U. Agrawal, J. Follum, J. W. Pierre, and D. Duan, "Electromechanical mode estimation in the presence of periodic forced oscillations," *IEEE Transactions on Power Systems*, vol. 34, no. 2, pp. 1579–1588, 2018.

[14] L. Dosiek, "The effects of forced oscillation frequency estimation error on the ls-arma+s mode meter," *IEEE Transactions on Power Systems*, vol. 35, no. 2, pp. 1650–1652, 2020.

[15] J. Follum, U. Agrawal, and P. Etingov, "Evaluation of mode meters robust to forced oscillations using field-measured data," *Proceedings of HICSS-54*, 2021.

[16] Z. Xu and J. W. Pierre, "Initial results for cramér-rao lower bound for forced oscillations in power systems," in *2021 North American Power Symposium (NAPS)*. IEEE, 2021, pp. 1–5.

[17] L. Dosiek, U. Agrawal, J. Follum, J. W. Pierre, and D. J. Trudnowski, "Analysis of power system mode meters under various oscillatory conditions," *2018 IEEE International Conference on Probabilistic Methods Applied to Power Systems (PMAPS)*, pp. 1–6, 2018.

[18] M. A. Khan and J. W. Pierre, "Detection of periodic forced oscillations in power systems using multitaper approach," *IEEE Transactions on Power Systems*, vol. 34, no. 2, pp. 1086–1094, 2018.

[19] J. Follum and J. W. Pierre, "Detection of periodic forced oscillations in power systems," *IEEE Transactions on Power Systems*, vol. 31, no. 3, pp. 2423–2433, 2015.

[20] M. A. Khan and J. W. Pierre, "Separable estimation of ambient noise spectrum in synchrophasor measurements in the presence of forced oscillations," *IEEE Transactions on Power Systems*, vol. 35, no. 1, pp. 415–423, 2020.

[21] J. Follum and J. Pierre, "Time-localization of forced oscillations in power systems," in *2015 IEEE Power & Energy Society General Meeting*. IEEE, 2015, pp. 1–5.

[22] S. M. Kay, *Fundamentals of statistical signal processing: estimation theory*. Prentice-hall Englewood Cliffs, NJ, 1993, vol. 1.